Available online at www.sciencedirect.com
SCIENCE DIRECT®
Catalysis Today 85 (2003) 113–124
CATALYSIS TODAY
www.elsevier.com/locate/cattod

Understanding silica-supported metal catalysts: Pd/silica as a case study

B.K. Min, A.K. Santra[1], D.W. Goodman*

Department of Chemistry, Texas A&M University, P.O. Box 30012, College Station, TX 77842-3012, USA

Received 4 April 2003; received in revised form 20 May 2003; accepted 30 May 2003

Abstract

Supported metal catalysts, particularly noble metals supported on SiO_2, have attracted considerable attention due to the importance of the silica–metal interface in heterogeneous catalysis and in electronic device fabrication. Several important issues, e.g., the stability of the metal–oxide interface at working temperatures and pressures, are not well-understood. In this review, the present status of our understanding of the metal–silica interface is reviewed. Recent results of model studies in our laboratories on Pd/SiO_2/Mo(1 1 2) using LEED, AES and STM are reported. In this work, epitaxial, ultrathin, well-ordered SiO_2 films were grown on a Mo(1 1 2) substrate to circumvent complications that frequently arise from the silica–silicon interface present in silica thin films grown on silicon.

Keywords: Metal clusters; Supported catalysts; Oxide; Metal–support interaction; SMSI; STM; Palladium; Silica; Films; Inter-diffusion; Silicide; Alloying and sintering

1. Introduction

The study of metal particles on oxide supports is of importance in heterogeneous catalysis because the size and nature of the interaction of a metal particle with an oxide support are critical in determining catalytic activity and selectivity [1–3]. It is well-known that metals on reducible oxides such as TiO_2 [4,5] exhibit a strong metal–support interaction (SMSI). On the other hand, irreducible oxides like SiO_2 are assumed to be relatively inert. However, in certain cases, silica has been shown to exhibit a metal–support interaction following a high temperature treatment [6–8].

Oxidation and reduction at elevated temperatures are essential steps for the preparation of supported, high surface area catalysts; however, these treatments can cause morphological changes of the dispersed metal particles arising from sintering and/or metal–support interactions. Therefore, it is of considerable importance to investigate and define optimal conditions for catalyst preparation, pretreatment and activation [9]. Depending on the particular metal–oxide system, various morphological changes resulting from a metal–support interaction have been reported, namely sintering [10–14], encapsulation [15,16], inter-diffusion [17–27], and alloy formation [28,29]. In particular, silicide formation from metals supported on silica has received considerable attention because of the importance of the metal–silica interface

* Corresponding author. Tel.: +1-979-845-6822; fax: +1-979-845-0214.
E-mail address: goodman@mail.chem.tamu.edu (D.W. Goodman).
[1] Present address: Halliburton Energy Services, Duncan, OK, USA.

0920-5861/$ – see front matter © 2003 Published by Elsevier B.V.
doi:10.1016/S0920-5861(03)00380-8

to numerous technologies. For example, studies of metal–oxide–semiconductor (MOS) structures are directly related to many aspects of semiconductor technology including the design of MOS devices. In addition, metallization is important for creating contact layers and durable electrically conducting vias on insulating substrates for semiconductor devices [30,31]. Furthermore, silicide formation between metals and SiO_2 in a catalyst has been shown to alter catalytic activity and selectivity [32,33]. For instance, it has been shown that Pd-silicide, formed during the high temperature reduction of Pd/SiO_2, dramatically increases selectivity for the isomerization of neopentane [33].

However, in spite of the numerous studies on metals supported on SiO_2 at elevated temperatures, there are still controversial and unresolved issues regarding the nature of the metal–support interaction in silica-supported catalysts, namely:

- the nature of the metal–support interaction between metals and SiO_2;
- the morphological changes that occur during the high temperature reduction of metals supported on SiO_2;
- the role of oxygen vacancies in the inter-diffusion of metals into SiO_2;
- the extent to which silicides are formed by the direct interaction between metals and SiO_2;
- the role of the silicon substrate, frequently used to prepare SiO_2 thin films, in metal silicide formation;
- the composition, if formed, of metal silicides;
- the mechanism of silicide formation between metals and SiO_2.

In the first section of this review, the effect of high temperature reduction of technical catalysts consisting of metals supported on high surface area SiO_2 will be discussed. In the second section, related results obtained for model catalyst systems will be described. Finally, recent studies from our laboratories for model SiO_2-supported Pd catalysts, consisting of SiO_2 thin films prepared on a Mo substrate, will be addressed and serve to illustrate how this particular model preparation circumvents the complications frequently encountered when using a silicon substrate to synthesize a thin film silica support.

2. Experimental

Details of the ultrahigh vacuum chamber, equipped with scanning tunneling microscope (STM), X-ray photoelectron spectroscopy (XPS), low energy electron diffraction (LEED), and Auger electron spectroscopy (AES) with a base pressure of 5×10^{-10} mbar, have been published elsewhere [34]. Briefly, this apparatus is equipped with a double-pass cylindrical mirror analyzer, reverse view LEED optics, and a room temperature STM (Omicron). Typically, the STM images were acquired in the constant current mode with a $\sim$2 V tip bias and a tunneling current of $\sim$0.1 nA. Ultrahigh purity (99.999%) oxygen from MG industries was used. A Mo(1 1 2) crystal, oriented with an accuracy of $<0.25^\circ$ (from Matek), was cleaned by flashing to 2100 K until no evidence of carbon and oxygen was detectable by AES. A W–5% Re/W–26% Re thermocouple was used to calibrate an optical pyrometer (OMEGA OS3700) that was then employed to monitor the crystal temperature during the STM experiments.

3. Results and discussion

3.1. High surface area, silica-supported metal catalysts

Reduction at elevated temperature is one of the important steps in the synthesis of supported metal catalysts; however, heating a supported metal catalyst can cause morphological changes in the metal particles depending upon the particular metal–oxide system. Chang et al. [9] have shown that various metal–support interactions are operative for Pd catalysts on various supports, e.g. SiO_2, Al_2O_3, and TiO_2, using a combination of temperature-programmed reduction and adsorption methods. Hydrogen adsorption experiments by this group on a SiO_2-supported Pd catalyst (1% Pd/SiO_2) showed no significant SMSI interaction even after heating to temperatures as high as 873 K. These results differ markedly from the data obtained for Pd/TiO_2 where a significant reduction of adsorbed hydrogen was attributed to a strong metal–support interaction. The SMSI was attributed to arise via the diffusion of partially reduced TiO_2 onto the surface of the Pd clusters. Based on these studies, the authors

suggested that the tendency for SMSI to occur between dispersed Pd and a support increases in the order: $Pd/SiO_2 < Pd/Al_2O_3 < Pd/TiO_2$. In addition, it was also suggested that Pd/SiO_2 displayed the least tendency to sinter compared with other metal–oxide pairs under identical reduction conditions.

Negligible sintering of Pd/SiO_2 (0.5–25.0% Pd) was reported by Moss et al. [35], who measured the Pd surface area by chemisorption of CO and H_2 following two reduction temperatures, 573 and 723 K. Electron micrographs of the Pd/SiO_2 catalysts corresponding to each reduction temperatures confirmed that no change has occurred in the metal morphology or dispersion; however, the specific catalytic activity for benzene hydrogenation dramatically decreased with an increase in the reduction temperature to 823 K. Three explanations for this were proposed: (i) a variation in the surface structure of the support, (ii) promoters or inhibitors on the Pd or the support, and (iii) an interaction between the Pd clusters and the support. The latter explanation was based on an X-ray diffraction investigation that indicated formation of a Pd–silicon intermetallic compound.

Direct evidence of Pd-silicide formation due to high temperature reduction has been suggested by Shen et al. [32,33]. Their XRD data of a mechanical mixture of Pd powder and silica gel after high temperature reduction (873 K) showed the presence of a Pd_3Si species. These authors suggested that the formation of this Pd-silicide species is responsible for the dramatic increase in the selectivity of this catalyst for the isomerization of neopentane. The silicide formation is believed to occur during high temperature reduction by diffusion of Pd atoms into the bulk via oxygen vacancies in the SiO_2. Pure Pd, however, was easily regenerated by the oxidation of the silicide at low temperature.

A change in catalytic activity following high temperature reduction has also been observed for Ni/SiO_2 and Pt/SiO_2. Martin et al. [36–39], have shown that the catalytic activity of Ni/SiO_2 (24% of Ni) for ethane hydrogenolysis and benzene hydrogenation decreases by an order of magnitude with an increase in the reduction temperature from 920 to 1120 K. Based on hydrogen chemisorption it was anticipated that reduction at high temperature would lead to sintering of the nickel particles, however, the effects were much larger than that expected from a simple increase in particle size. A similar but more significant effect of high temperature reduction was also observed for a Pt/SiO_2 catalyst.

3.2. Model silica-supported metal catalysts

3.2.1. Sintering

Sintering [40–43] can be understood using the Gibbs–Thompson relationship where larger particles with lower chemical potential will grow at the expense of smaller particles with higher chemical potential, the driving force being the reduction of the total surface energy of the system. Sintering is certainly affected by the environment and can be accelerated by a reactant gas and by temperature. In addition, sintering is strongly dependent on the nature of the metal–support interaction, i.e., the relative strengths of the metal–metal versus the metal–support bond energies. Generally, it is believed that for metals on an irreducible oxide support, the strength of the metal–metal bond is significantly larger than the metal–support bond, leading to a relatively weak metal–support interaction and facile thermal sintering.

Pretorius et al. [10] have investigated the interaction between various metals including noble metals and SiO_2 thin films at high temperature (1073 K) using Rutherford backscattering (RBS) and scanning electron microscopy (SEM). Their results show that metals do not react with a SiO_2 substrate whereas Ti, Zr, Hf, V, and Nb do react to form metal silicides. SEM images also have confirmed that islands of metals tend to coalesce with a high temperature anneal. For noble metals, heats of formation were calculated and found to be positive using the following reaction: $M + SiO_2 \rightarrow MSi_x + MO_y$. It was also suggested that these heats of formation should correlate with the mean electronegativity of the metal, allowing the relative reactivity of a metal with SiO_2 to be predicted. With these considerations, metals with an electronegativity of less than 1.5 on the Pauling scale should react with a SiO_2 substrate; the values for noble metals fall within the range 1.67–1.80, and therefore these metals should be unreactive [10].

Chen and Schmidt [11] have investigated the effects of reactive gases and temperature on the sintering rates and morphology of Pt particles on amorphous SiO_2. Using transmission electron microscopy the average crystallite size of the Pt particles increased dramatically when heated to 973 K.

The structure and chemical properties of model silica-supported metal catalysts have been investigated in our laboratory using various surface science techniques [12–14,44–46]. SiO_2 thin films were prepared by high temperature co-deposition of Si and oxygen onto a Mo(1 1 0) or Mo(1 0 0) substrate followed by an anneal, a procedure that yields an amorphous oxide film. Temperature-programmed desorption (TPD) experiments for the Cu/SiO_2 system showed that the saturation coverage of CO decreases by a factor of 2 with an increase in the annealing temperature from 100 to 900 K. In addition, marked changes in infrared reflection adsorption spectra (IRAS) were also observed. Fig. 1 shows IRAS of CO on silica-supported Cu as a function of the pre-anneal temperature. On the as-deposited (100 K) Cu clusters, CO exhibits an IR absorption band centered at 2099 cm^{-1} with a small shoulder on the low-frequency side of the peak. Upon annealing to 300–500 K the 2099 cm^{-1} band shifts to 2097 cm^{-1}, and a new band appears at 2070 cm^{-1}. Further heating to 700–900 K results in a splitting of the 2097 cm^{-1} feature into two peaks at 2018 and 2094 cm^{-1}. These CO absorption bands are attributed to several distinct atop CO adsorption sites implying CO adsorption onto various Cu crystalline facets. TPD for CO adsorption at 90 K on Cu/SiO_2 annealed to 1200 K shows no evidence for CO adsorption even though Cu is still evident on the surface as evidenced by the Cu TPD of Fig. 2. The β-peak at 1000 K was assigned to metallic Cu; the α-peak (1300 K) was attributed to a Cu species strongly bonded to the SiO_2 surface since its desorption temperature was 200 K higher than the bulk Cu sublimation temperature. In addition, no adsorption of CO on Cu/SiO_2, pre-annealed to 1200 K, indicated that this high temperature Cu species is not metallic in nature.

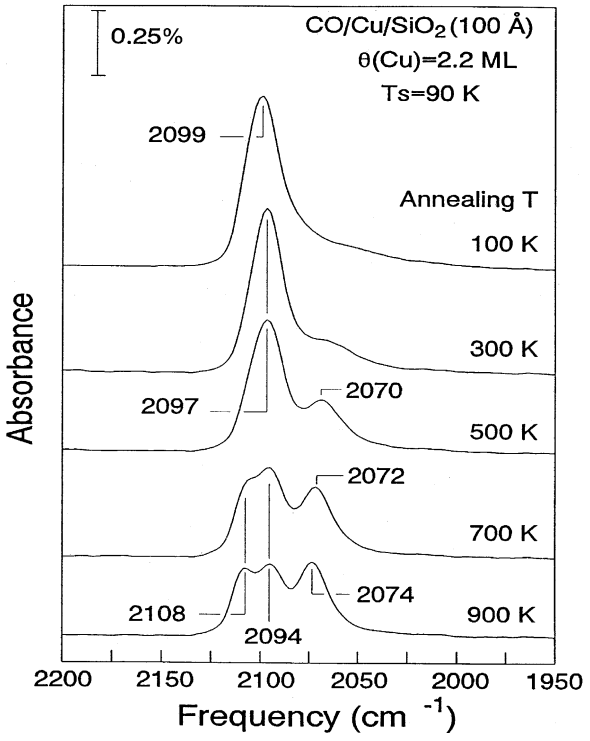

Fig. 1. IRAS of CO on silica-supported Cu as a function of the pre-annealing temperature. Cu was deposited at 100 K and annealed to the indicated temperatures, followed by CO adsorption to saturation at 90 K.

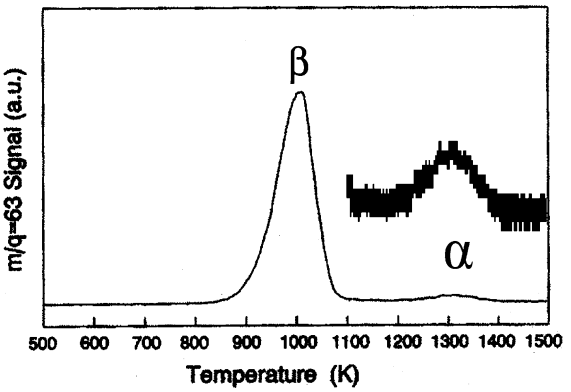

Fig. 2. TPD from $Cu/SiO_2/Mo(1\,1\,0)$. The silica film is ~10 nm thick and the Cu coverage is $\sim 8 \times 10^{14}$ atoms/cm^2 (~0.6 MLE). The silica film was annealed to 1500 K before Cu deposition. Cu was deposited at 90 K and the heating rate for TPD was 10 K/s.

The surface structure of supported Pd clusters on similarly prepared silica films was also investigated with IRAS of adsorbed CO. As shown in Fig. 3, for the as-deposited Pd film, two broad bands were observed at 2110 and 1990 cm^{-1}, corresponding to CO adsorption on atop and bridging sites, respectively. Annealing the films to >500 K leads to a new band at 1890 cm^{-1}, that corresponds to CO adsorbed on threefold hollow sites [14]. In addition, the peak for the atop and bridging bands becomes much sharper for the annealed films. This narrowing of the peaks is attributed to the formation of stable, extended facets. Fig. 4 shows the oxygen TPD from $O/Pd/SiO_2$.

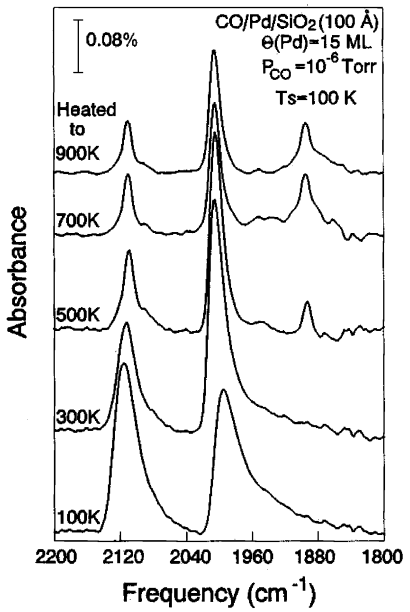

Fig. 3. IRAS of CO on a model silica-supported Pd catalyst ($\theta_{Pd} = 15$ MLE) as a function of pre-annealing temperature. The spectra were collected at 100 K and in 10^{-6} Torr CO background. The surface was annealed to 100, 300, 500, 700 and 900 K, respectively.

Oxygen desorption occurs primarily within the temperature range 700–900 K, similar to oxygen desorption from Pd single crystals and foils. In addition, a small oxygen desorption peak is observed between 1200 and 1300 K, the temperature range within which Pd is known to sublime. This high temperature oxygen desorption feature is attributed to oxygen absorbed within the bulk of the Pd clusters. However, oxygen desorption via decomposition of the silica film at high temperature catalyzed by Pd is also a possibility; this point will be discussed later in the text.

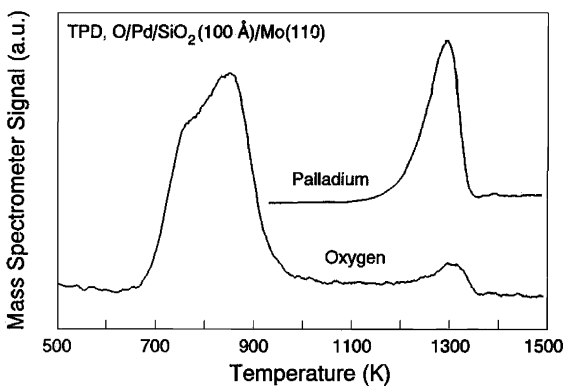

Fig. 4. TPD from O/Pd/SiO_2/Mo(1 1 0). The Pd coverage is 6×10^{15} atoms/cm^2. Oxygen was adsorbed at 100 K to saturation.

3.2.2. Encapsulation

One deactivation mechanism for supported metal catalysts is encapsulation [1,15] resulting in a reduction in the active metal surface area. This decrease in the ratio of the metal surface area to the metal interface area occurs when hemispherical metal clusters on an oxide surface are partially encapsulated by the oxide support. Powell and Whittington [15] first proposed encapsulation to account for the change in morphology of silica-supported platinum model catalysts following a high temperature anneal. These authors, using SEM, showed that Pt particles became partially immersed in the SiO_2 surface with concomitant formation of a SiO_2 ridge around the base of the Pt particles when annealed at 1200 and 1375 K.

Recently, Van den Oetelaar et al. [16,28] have investigated the metal–support interaction between Cu and SiO_2 using LEIS, AFM, and RBS by preparing very thick SiO_2 films (400–500 nm) on a silicon wafer. The LEIS measurements showed that the coverage of Cu gradually decreased following an anneal to 773 K and completely disappeared after an anneal to 923 K indicating that no bare Cu remained on the surface. The RBS data, however, were unchanged following an anneal to 923 K, consistent with encapsulation of the Cu clusters.

3.2.3. Inter-diffusion

Numerous investigations have shown that metals can diffuse into a SiO_2 support. Scott and Lau [17] have investigated the effects of interfacial SiO_2 on the formation of a metal silicide with a silicon substrate using RBS and $^{16}O(d,\alpha)^{14}N/^{18}O(d,\alpha)^{15}N$ nuclear reactions. A SiO_2 layer was synthesized on a silicon wafer by oxidation, then a noble metal, e.g. Pd, Pt, Ni, evaporated onto it. A feature corresponding to a metal silicide was observed at the interfacial region of SiO_2 after an anneal to 673–1023 K. As a plausible explanation, the authors suggested the following. Initially, the SiO_2 is present as a layer between the metal and the silicon. Upon annealing at a sufficiently high temperature, the metal diffuses through the SiO_2 layer

to form a silicide. The formation of the silicide gives rise to lateral non-uniformities in the layer such that the barrier to silicon diffusion is significantly lowered, i.e., silicon diffusion, no longer blocked by the SiO_2 layer, is facilitated.

Schleich et al. [18] have also investigated Pd-silicide formation on oxidized Si(1 1 1) using XPS and HREELS. These authors showed that a loss feature related to a C–O vibration near 240 mV disappeared after annealing to >510 K implying the disappearance of Pd on SiO_2. Furthermore, subsequent to a 820 K anneal, the HREELS spectrum showed a feature similar to that acquired from a freshly prepared SiO_2 surface. In addition, XPS spectra showed an additional feature after a 600 K anneal near 336.9 eV in addition to the feature related to Pd^0. This additional feature was consistent with the formation of Pd-silicide; silicide formation was confirmed by XPS spectra following an anneal of Pd on a clean Si(1 1 1)-7 × 7 surface. Based on these results these authors concluded that annealing leads to diffusion of Pd to the Si/SiO_2 interface, likely via oxygen vacancies. At the interface, elemental silicon is available for reaction with Pd to form Pd_2Si.

Anton et al. [19,20] have investigated the growth of Pd on thermally grown or native silica layers at high temperature using AES, reflection high energy electron diffraction, SEM, and Auger sputter profiling. In this study, the decrease of the metal AES intensity following an anneal to 893 K was interpreted as due to diffusion of metal clusters into the oxide layer. Moreover, an Auger sputter profile of oxide-supported Pd showed Pd-silicide formation subsequent to an anneal to 893 K. These authors concluded that the interaction between Pd and silicon oxide is much more pronounced for a native oxide interface than for a thermally grown oxide due to the differences in stoichiometry.

The morphological change of Ni clusters on thermally grown SiO_2 on a silicon wafer as a function of temperature has been systematically studied by Mayer et al. [21], using XPS, HREELS, LEED, AFM, and metastable impact electron spectroscopy (MEIS). Plots of Ni $2p_{3/2}$ XPS intensity and the relative height of the silica phonon peaks from HREELS versus temperature showed two distinct regions indicating that two distinct morphologies occur on Ni/SiO_2 with a change in temperature. The first HREELS region (100–850 K) indicated a gradual attenuation of the Ni $2p_{3/2}$ XPS intensity accompanied by a slow increase in the height of the silica phonon peaks as a function of temperature, consistent with sintering of the Ni clusters. However, in the second region (700–1050 K), a very rapid decrease in the Ni $2p_{3/2}$ intensity with an increase in the height of the silica phonon peaks from HREELS was observed yielding a breakpoint at 850 K. Inter-diffusion of Ni clusters into the bulk was invoked to explain the experimental results within this latter temperature region. In addition, Ni silicide formation was observed above 950–1100 K and was accompanied by decomposition and desorption of the oxide layers.

Dallaporta et al. [26,27] have studied the thermal stability of SiO_2 films on Si(1 0 0) induced by various metals during a vacuum anneal using scanning Auger microscopy (SAM) and SEM. These authors observed metal-induced decomposition of the SiO_2 films and proposed two possible mechanisms, each with a varying dependence on the electronic properties of the metal. One metal type, corresponding to s-type, p-type, and transition metals with few d electrons, react directly with SiO_2 and lead to homogeneous decomposition. Metals, on the other hand, must diffuse to the interface likely via defects where heterogeneous decomposition occurs. Furthermore, the authors suggest that decomposition of SiO_2 by a noble metal is generally exothermic. This excess energy then assists the further reaction of SiO_2 and Si to SiO, thereby enhancing the defect concentration. Alternatively, the altered electronic structure of the metal subsequent to reaction could facilitate the breaking of the Si–O bond.

3.2.4. Alloy formation

Considerable work, some already discussed, has shown metal silicide to form between a metal and silica grown on a silicon wafer. In general, it is believed that oxygen vacancies are the primary diffusion pathways for the formation of silicide at the interface between SiO_2 and Si. However, studies have shown that metal silicide formation can occur via direct interaction between SiO_2 and the metal.

As discussed above [16,28], temperature dependent AES studies of Cu supported on thick films of SiO_2 (400–500 nm, in order to avoid any influence of underlying Si) clearly show splitting of the Si LVV peak at 92 eV into two peaks at 90 and 94 eV, respectively,

due to Cu-silicide formation. Furthermore, this silicide feature in the AES was enhanced with an anneal at 893 K.

Very recently, the thermal stability of Pd supported on single crystalline SiO_2 thin films grown on Mo(1 1 2) substrate has been investigated in our laboratory using STM and AES techniques. In this work, a Mo substrate rather than a Si substrate was used to support a SiO_2 thin film to avoid complications of silicide formation at the Si–SiO_2 interface. Well-ordered, epitaxial SiO_2 ultrathin films (∼0.4 nm) have been prepared on a Mo(1 1 2) surface in two different ways: (a) vapor deposition of Si onto a Mo(1 1 2) single crystal followed by oxidation and high temperature annealing [47] and (b) vapor deposition of Si onto a (2 × 3)-O oxygen reconstructed Mo(1 1 2) surface followed by oxidation and annealing [48,49]. A typical STM image of SiO_2 ultrathin films prepared by the above methods are shown in Fig. 5a (film I) and d (film II), respectively, showing wide terraces and steps consistent with the underlying Mo(1 1 2) substrate. Also, both films show a sharp hexagonal LEED pattern confirming the long-range order of the film; STS as well as MIES and UPS data [50] indicate a wide band gap (∼9 eV) and confirm the bulk-like electronic character of the SiO_2 surface. However, STM images of film I show a more defective and less uniform surface compared with film II. The STM images of Fig. 5b and e show the nucleation and growth behavior of Pd clusters (∼2 monolayer equivalents (MLE)) on these two different SiO_2 thin films (I and II) at room temperature. Fig. 5b show elongated, hemispherical particles at high density and with diameter of 2–3 nm distributed homogeneously on the surface. In Fig. 1e larger Pd clusters (3–6 nm), distributed less densely, are evident. It is generally believed that metal particles nucleate and grow preferentially on point defects on oxide surfaces, presumably at oxygen vacancies [51]. Therefore, the higher number density of the Pd clusters in film I than that of film II suggests a more highly defective surface.

The STM images acquired after annealing to 700 K show no appreciable change with respect to cluster size or shape for either film I or II. However, those images acquired after annealing to 1000 K (Fig. 5c and f), show marked changes. The Pd clusters on the more defective SiO_2 surface (film I), rather than being 3D, have spread on the SiO_2 surface. The Pd clusters on the less defective SiO_2 surface (film II) exhibit an elongated rectangular shape with increasing size, a decrease in the number density, and a decrease in the cluster height. The total volume of Pd particles calculated from STM images shows a ∼20% decrease. This decrease is not due to desorption of Pd since desorption of Pd takes place above 1050 K. It is also quite clear that under our experimental conditions Pd particles on both SiO_2 films remain morphologically unperturbed until 700 K, however, clusters on film II sinter between 750 and 1000 K; this sintering is accompanied by inter-diffusion. On the other hand, the behavior observed on film I shows a dramatic change in morphology. For reference, the surface of Fig. 1c will be designated “activated”, and the specifics of this surface will be addressed subsequently.

In order to investigate the thermal stability of the Pd/SiO_2 system, annealing was carried out in a step-wise manner. Fig. 6 shows changes in the relative AES intensity ratios of I_{Pd}/I_{Mo} (a) and I_O/I_{Mo} (b) during these annealing experiments. Consistent with the STM results, no changes in I_{Pd}/I_{Mo} or I_O/I_{Mo} are observed at temperatures to 700 K. However, between 750 and 1050 K, the ratios I_{Pd}/I_{Mo} decrease while the ratios I_O/I_{Mo} remain unchanged. Above 1050 K, a marked decrease in I_O/I_{Mo} occurs and is accompanied by a decrease in I_{Pd} and I_{Si}. From previous work in our laboratories, desorption of Pd was shown to began at ∼1050 K whereas the onset of the decomposition of the SiO_2 thin films occurs at ∼1200 K. Therefore, the concomitant loss of oxygen and silicon above 1050 K in Fig. 2 is likely due to Pd-induced decomposition of the SiO_2 thin film, either involving the formation of a volatile Pd-silicide or SiO/Si, concurrent with Pd desorption since no characteristic feature of silicide (splitting of the Si LVV peak at 92 eV into two peaks at 90 and 94 eV) was detected by AES.

As mentioned earlier, in Pd/SiO_2 high surface area catalysts, evidence for Pd_3Si formation has been reported using XRD subsequent to hydrogen reduction at 873 K [33]. In addition, it has also been suggested that point defects on SiO_2 thin films are the primary mechanism for inter-diffusion of Pd. In order to investigate the role of point defects, a defective surface was prepared by electron beam bombardment. An electron beam produced a new feature at 92 eV, whose intensity grows with exposure time. This feature is assigned to a Si^0 species arising from SiO_2 + e-beam →

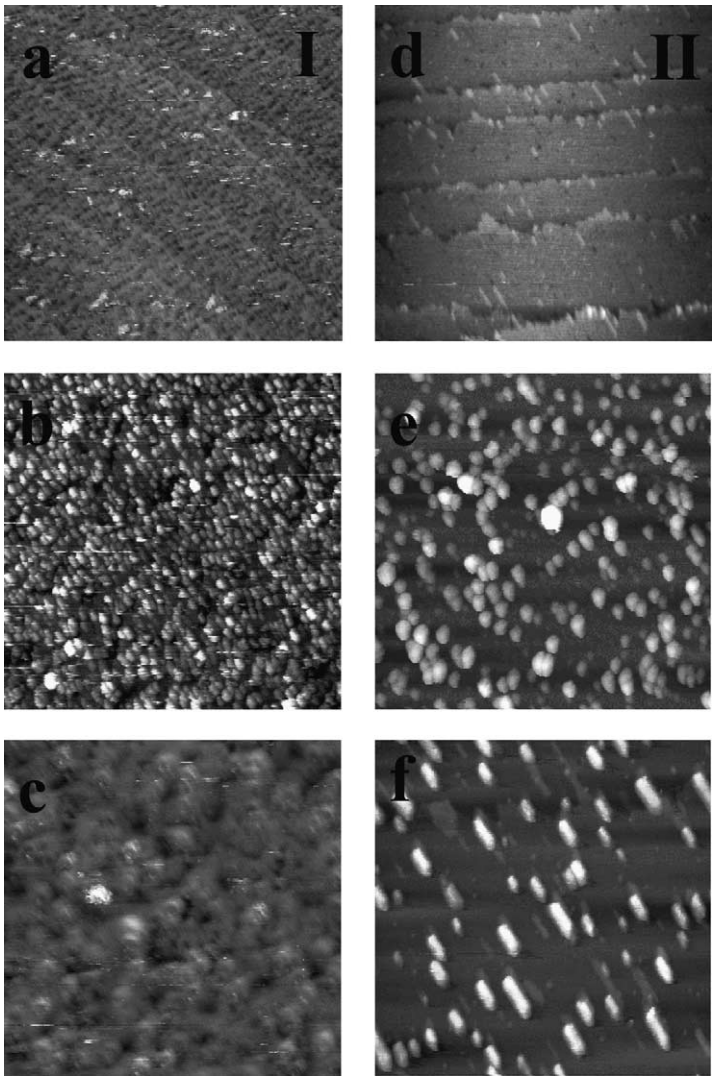

Fig. 5. STM images of: (a) a clean SiO_2 thin film (200 nm × 200 nm) with a thickness of ∼0.4 nm (considered to be the more defective surface); (b) ∼2 MLE Pd on SiO_2 thin film (a) (100 nm × 100 nm) at room temperature; (c) activated Pd surface (100 nm × 100 nm) taken after a 1000 K anneal of (b); (d) a clean SiO_2 thin film (200 nm × 200 nm) with the thickness of ∼0.4 nm (considered to be the less defective surface); (e) ∼2 MLE Pd on SiO_2 thin film (c) (100 nm × 100 nm) at room temperature and (f) Pd surface (100 nm × 100 nm) taken after a 1000 K anneal of (e).

$Si^0 + O_2$ (g) reaction. However, step-wise annealing, subsequent to the deposition of Pd and annealing below 1000 K followed by deposition of elemental Si, showed no evidence of Pd-silicide, even though Si/Pd and Pd/Si are known to mix readily at this temperature [52–55]. This suggests that Si and Pd nucleate separately on the SiO_2 surface. It is also noteworthy that the deposition of elemental Si on Pd on less defective SiO_2 thin film (Fig. 5f) does not produce a silicide feature.

However, point defects, created by electron beam bombardment on an "activated" Pd/SiO_2 surface (as shown in Fig. 5c), lead to silicide formation upon annealing to 1000 K (AES spectrum shown in Fig. 7a). According to the detailed AES study of Tanaka et al. [56], this silicide is Pd-rich. Alternatively, upon

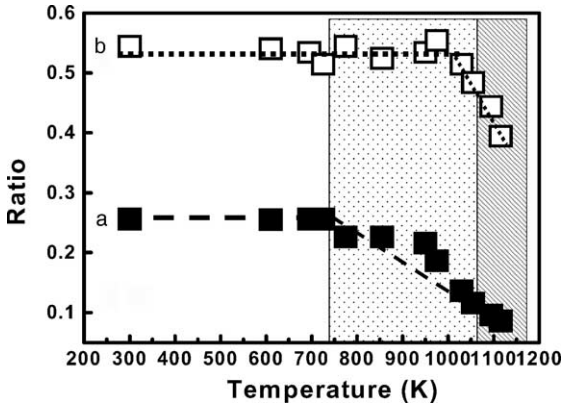

Fig. 6. The plots of AES intensity ratio as a function of annealing temperature: (a) I_{Pd}/I_{Mo} and (b) I_O/I_{Mo}.

deposition of 0.5 MLE of Si onto an activated Pd/SiO_2 surface, a silicon-rich silicide was observed after annealing to 1000 K (Fig. 7b(1)). An even greater silicon-rich silicide was observed (Fig. 7b(2)) following the deposition of 1.0 MLE Si and an anneal to 1000 K. In other words, the composition of the silicide depends on the amount of pre-adsorbed silicon. It is noteworthy that significant loss of oxygen is evident during silicide formation due to the decomposition of SiO_2.

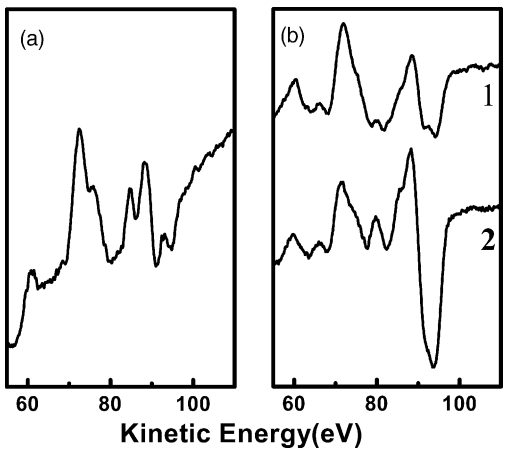

Fig. 7. High resolution AES spectra around Si LVV peak (55–110 eV) region. The splitting of the Si LVV peak at 92 eV into two peaks at 90 and 94 eV indicates silicide feature. (a) Silicide formation induced by point defects from electron beam bombardment and (b) silicide formation induced by (1) 0.5 MLE pre-deposited Si and (2) 1.0 MLE pre-deposited Si.

Based on these observations, the following conclusions can be drawn: (a) an "activated" surface is essential for low temperature silicide formation and (b) deposited Si or point defects created by electron beam bombardment aid in the production of silicide at temperatures between 850 and 1000 K as detected by AES. It is also noteworthy that it is possible to reversibly re-oxidize the silicide-containing surface by treatment in 1×10^{-5} mbar of oxygen for 1 h at room temperature.

In order to understand the role of Si in the formation of Pd-silicide, step-wise annealing experiments were carried out after depositing a trace of silicon on an "activated" Pd/SiO_2 surface. As shown in Fig. 8(a) the amount of silicide increases with the anneal time and is accompanied by loss of oxygen (Fig. 8b(1)). Silicide formation also induces an increase in the AES intensity ratio of I_{Pd}/I_{Mo} (Fig. 8b(2)), consistent with 2D silicide formation on the oxide and segregation of the volatile Pd-silicide to the surface. Based on these results the amount of silicide formed does not depend on the amount of Si deposited, but rather on the annealing time. In other words, a trace of Si acts as an initiator for this reaction. An excess of Si accelerates the reaction and alters the composition of the silicide product.

The nature of the "activated" surface has been studied by STM. Fig. 9a–c shows STM images of a

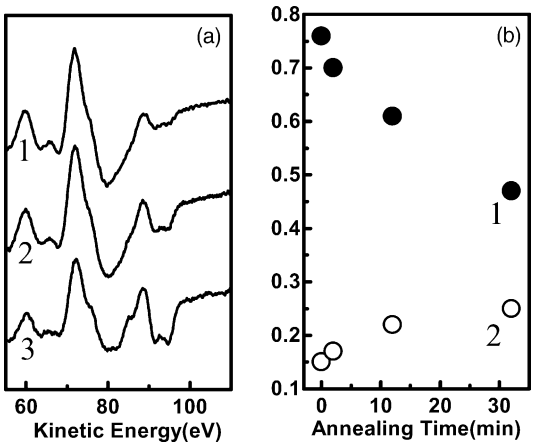

Fig. 8. (a) High resolution AES spectra near the Si LVV region as a function of annealing time at 1000 K where spectrum 1, 2 and 3 correspond to 2, 12 and 32 min, respectively. (b) A plot of AES intensity ratio as a function of annealing time at 1000 K: (1) I_O/I_{Mo} and (2) I_{Pd}/I_{Mo}.

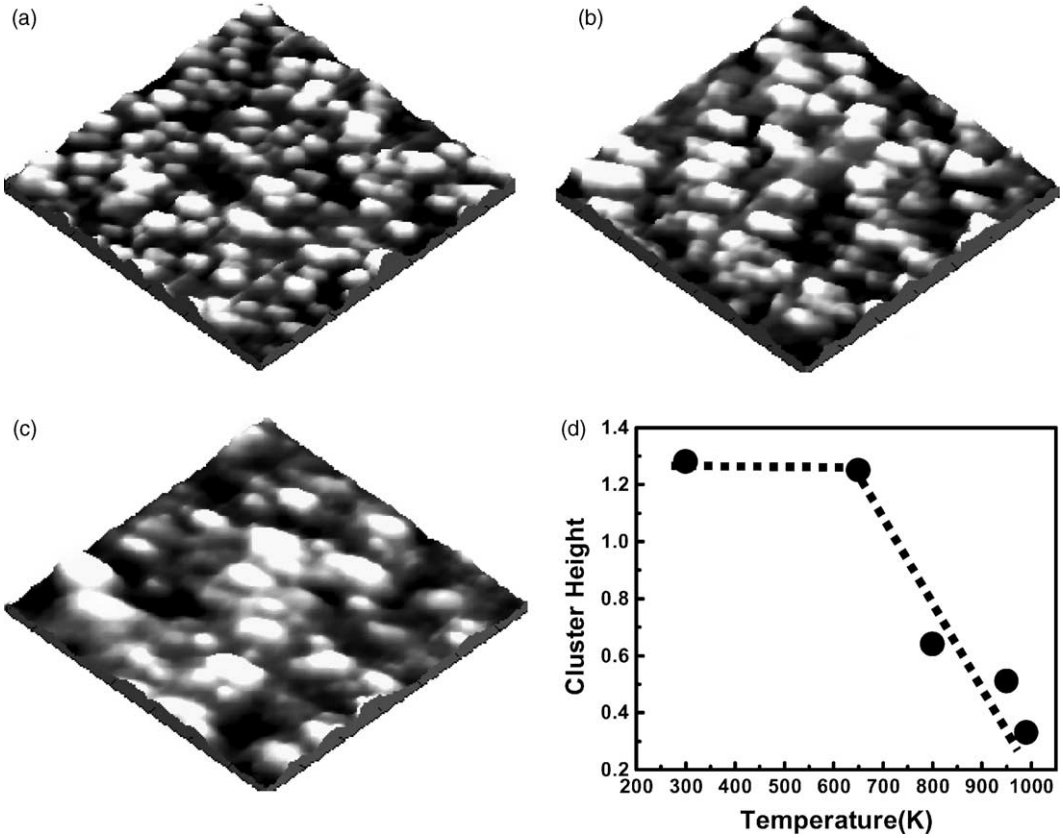

Fig. 9. STM images (34 nm × 34 nm) in 3D-view of Pd/SiO_2 surfaces acquired after annealing at (a) 300, (b) 800 and (c) 950 K, respectively. Plot (d) shows change in the average height of the clusters as a function of the annealing temperature.

Pd/SiO_2 surface following anneals at 300, 800, and 950 K, respectively. As discussed earlier, no changes in the cluster shape and size are apparent until approximately 700 K. However, it is clear from the images of Fig. 9a–c that the number density of the Pd clusters decreases while the diameter of the Pd clusters increases with an increase in the annealing temperature above 750 K. Fig. 5d shows how the average height of the clusters (calculated from the corresponding STM image) changes with respect to the annealing temperature. These results imply that Pd sintering and inter-diffusion occur simultaneously with an increase in the anneal temperature as shown schematically in Fig. 10.

Simple thermodynamic considerations preclude the reaction pathway: $Pd + Si_yO_2 \rightarrow PdSi_y + O_2\,(g)$. However, for the Cu/SiO_2 system, Van den Oetelaar

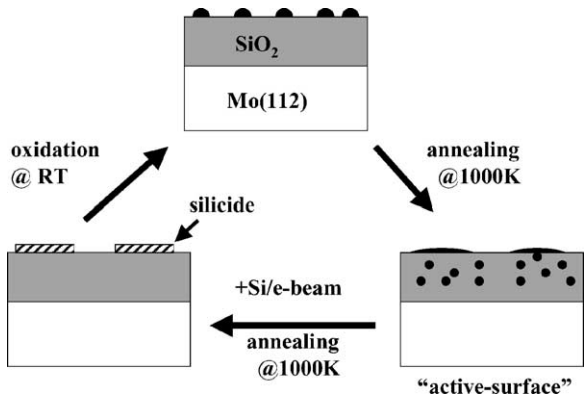

Fig. 10. Schematic diagram of proposed model for Pd-silicide formation.

et al. [16] have suggested that the formation of a $Cu^{\delta+}$ species, due to the interaction between the Cu and the support, could alter the surface/interface free energies such that reaction between the SiO_2 support and Cu at high temperature can occur. In the present system only the "activated" surface forms silicide via reaction with surface defects (e-beam-induced as well as via deposition of Si) prior to desorption as metallic Pd. Therefore, by analogy to the Cu/SiO_2 system, it is likely that Pd in Pd/SiO_2 is present as $Pd^{\delta+}$. This relatively strong interaction between Pd and defects on SiO_2 explains the nucleation of Si on Pd/SiO_2 systems. For the non-activated system, Pd and Si nucleate separately and thus do not mix below the desorption temperature of Si. On the other hand, for the "activated" surface, the presence of $Pd^{\delta+}$ can preferentially lead to the adsorption of Si on or very near to the highly dispersed Pd followed by the formation of a silicide.

4. Conclusions

It has been shown that metals supported on SiO_2 exhibit a metal–support interaction that varies from weak to strong, depending upon the metal, after high temperature treatments. A strong metal–support interaction, manifested as encapsulation, inter-diffusion, and alloying, can alter the catalytic property significantly. In general, sintering is favored in those systems that show a weak metal–support interaction whereas encapsulation or/and inter-diffusion and alloy formation occurs for the strongly interacting systems. By using ultrathin, well-ordered SiO_2 films prepared on Mo(1 1 2), the interference of the under-lying substrates, particularly Si, can be excluded. More importantly, we have shown that defects, e.g. oxygen vacancies or excess Si, play a critical role in determining the strength of the metal–support interaction.

Acknowledgements

The authors acknowledge with pleasure the support of this work by the Department of Energy, Office of Basic Energy Science, and Division of Chemical Science, and the Robert A. Welch Foundation.

References

[1] S.A. Stevenson, R.T.K. Baker, J.A. Dumesic, E. Ruckenstein (Eds.), Metal–Support Interactions in Catalysis, Sintering, and Redispersion, Catalysis Series, Van Nostrand Reinhold, New York, 1987.
[2] M. Valden, X. Lai, D.W. Goodman, Science 281 (1998) 5383.
[3] M. Haruta, Catal. Today 36 (1997) 153.
[4] S.J. Tauster, S.C. Fung, R.L. Garten, J. Am. Chem. Soc. 100 (1978) 170.
[5] S.J. Tauster, S.C. Fung, R.T.K. Baker, J.A. Horsley, Science 221 (1981) 1121.
[6] A. Katrib, C. Petit, P. Legare, L. Hilaire, G. Maire, Surf. Sci. 189–190 (1987) 886.
[7] R. Lamber, N. Jaeger, G. Schulz-Ekloff, Surf. Sci. 227 (1990) 268.
[8] R. Lamber, W. Romanowski, J. Catal. 105 (1987) 213.
[9] T.-C. Chang, J.-J. Chen, C.-T. Yeh, J. Catal. 96 (1985) 51.
[10] R. Pretorius, J.M. Harris, M.-A. Nicolet, Solid-State Electron. 21 (1978) 667.
[11] M. Chen, L.D. Schmidt, J. Catal. 55 (1978) 348.
[12] X. Xu, J.-W. He, D.W. Goodman, Surf. Sci. 284 (1993) 103.
[13] X. Xu, D.W. Goodman, Appl. Phys. Lett. 61 (1992) 1799.
[14] X. Xu, J. Szanyi, Q. Xu, D.W. Goodman, Catal. Today 21 (1994) 57.
[15] B.R. Powell, S.E. Whittington, J. Catal. 81 (1983) 382.
[16] L.C.A. Van den Oetelaar, A. Partridge, S.L.G. Toussaint, C.F.J. Flipse, H.H. Brongersma, J. Phys. Chem. B 102 (1998) 9541.
[17] D.W. Scott, S.S. Lau, Thin Solid Films 104 (1983) 227.
[18] B. Schleich, D. Schmeisser, W. Gopel, Surf. Sci. 191 (1987) 367.
[19] R. Anton, U. Neukirch, M. Harsdorff, Phys. Rev. B 36 (1987) 7422.
[20] R. Anton, Thin Solid Films 118 (1984) 293.
[21] J.T. Mayer, R.F. Lin, E. Garfunkel, Surf. Sci. 265 (1992) 102.
[22] J.B. Zhou, T. Gustafsson, R.F. Lin, E. Garfunkel, Surf. Sci. 284 (1993) 67.
[23] S.M. Goodnick, M. Fathipour, D.L. Ellsworth, C.W. Wilmsen, J. Vac. Sci. Technol. 18 (1981) 949.
[24] R. Lamber, Thin Solid Films 128 (1985) L29.
[25] H. Praliaud, G.A. Martin, J. Catal. 72 (1981) 394.
[26] H. Dallaporta, M. Liehr, J.E. Lewis, Phys. Rev. B 41 (1990) 5075.
[27] M. Liehr, H. Dallaporta, J.E. Lewis, Appl. Phys. Lett. 53 (1988) 589.
[28] L.C.A. Van den Oetelaar, R.J.A. Van den Oetelaar, A. Partridge, C.F.J. Flipse, H.H. Brongersma, Appl. Phys. Lett. 74 (1999) 2954.
[29] B.K. Min, A.K. Santra, D.W. Goodman, J. Vac. Sci. Technol., in press.
[30] S.M. Sze, VLSI Technology, McGraw-Hill, New York, 1983.
[31] M. Liehr, H. Lefakis, F.K. Legoues, G.W. Rubloff, Phys. Rev. B 33 (1986) 5517.
[32] L.-L. Shen, Z. Karpinksi, W.M.H. Sachtler, J. Phys. Chem. 93 (1989) 4890.
[33] W. Juszczyk, Z. Karpinski, J. Catal. 117 (1989) 519.

[34] X. Lai, T.P. St. Clair, M. Valden, D.W. Goodman, Prog. Surf. Sci. 59 (1998) 25.
[35] R.L. Moss, D. Pope, B.J. Davis, D.H. Edwards, J. Catal. 58 (1979) 206.
[36] G.A. Martin, J.A. Dalmon, J. Catal. 75 (1982) 233.
[37] G.A. Martin, J.A. Dalmon, React. Kinet. Catal. Lett. 16 (1981) 325.
[38] G.A. Martin, R. Dutartre, J.A. Dalmon, React. Kinet. Catal. Lett. 16 (1981) 329.
[39] M. Primet, J.A. Dalmon, G.A. Martin, J. Catal. 46 (1977) 25.
[40] P. Wynblatt, N.A. Gjostein, Acta Metall. 24 (1976) 1165.
[41] C.H. Bartholomew, Appl. Catal. A 107 (1993) 1.
[42] H. Poppa, Thin Solid Films 34 (1976) 94.
[43] J.J. Chen, E. Ruckenstein, J. Catal. 69 (1981) 254.
[44] X. Xu, D.W. Goodman, J. Phys. Chem. 97 (1993) 683.
[45] X. Xu, S.M. Vesecky, D.W. Goodman, Science 258 (1992) 788.
[46] X. Xu, S.M. Vesecky, J.-W. He, D.W. Goodman, J. Vac. Sci. Technol. A 11 (1993) 1930.
[47] A.K. Santra, B.K. Min, D.W. Goodman, Surf. Sci. 515 (2002) L475.
[48] A.K. Santra, B.K. Min, D.W. Goodman, Surf. Sci. 513 (2002) L441.
[49] E. Ozensoy, B.K. Min, D.W. Goodman, J. Phys. Chem. B., submitted for publication.
[50] Y.D. Kim, T. Wei, D.W. Goodman, Langmuir 19 (2003) 354.
[51] A. Bogicevic, D.R. Jennison, Surf. Sci. 515 (2002) L481.
[52] B. Carriere, B. Lang, Surf. Sci. 64 (1977) 209.
[53] E. Kampshoff, N. Walchli, K. Kern, Surf. Sci. 406 (1998) 117.
[54] N. Walchli, E. Kampshoff, A. Menck, K. Kern, Surf. Sci. 382 (1997) L705.
[55] I.V. Lyubinetsky, V.K. Adamchuk, Thin Solid Films 288 (1996) 182.
[56] K. Tanaka, K. Furui, M. Yamada, J. Phys. Soc. Jpn. 64 (1995) 4790.